JACS JOURNAL OF THE AMERICAN CHEMICAL SOCIETY

Article

Cite This: J. Am. Chem. Soc. 2019, 141, 5995−6005

pubs.acs.org/JACS

Triptycene Tripods for the Formation of Highly Uniform and Densely Packed Self-Assembled Monolayers with Controlled Molecular Orientation

Fumitaka Ishiwari,[†,#] Giulia Nascimbeni,[§,#] Eric Sauter,[∥,#] Hiromu Tago,[†] Yoshiaki Shoji,[†] Shintaro Fujii,[⊥] Manabu Kiguchi,[⊥] Tomofumi Tada,[‡] Michael Zharnikov,[*,∥] Egbert Zojer,[*,§] and Takanori Fukushima[*,†]

[†]Laboratory for Chemistry and Life Science, Institute of Innovative Research, and [‡]Materials Research Center for Element Strategy, Tokyo Institute of Technology, 4259 Nagatsuta, Midori-ku, Yokohama 226-8503, Japan

[§]Institute of Solid State Physics, NAWI Graz, Graz University of Technology, Petersgasse 16, Graz 8010, Austria

[∥]Applied Physical Chemistry, Heidelberg University, Im Neuenheimer Feld 253, Heidelberg 69120, Germany

[⊥]Department of Chemistry, Graduate School of Science and Engineering, Tokyo Institute of Technology, Meguro, Tokyo 152-8551, Japan

Supporting Information

ABSTRACT: When employing self-assembled monolayers (SAMs) for tuning surface and interface properties, organic molecules that enable strong binding to the substrate, large-area structural uniformity, precise alignment of functional groups, and control of their density are highly desirable. To achieve these goals, tripod systems bearing multiple bonding sites have been developed as an alternative to conventional monodentate systems. Bonding of all three sites has, however, hardly been achieved, with the consequence that structural uniformity and orientational order in tripodal SAMs are usually quite poor. To overcome that problem, we designed 1,8,13-trimercaptomethyltriptycene (**T1**) and 1,8,13-trimercaptotriptycene (**T2**) as potential tripodal SAM precursors and investigated their adsorption behavior on Au(111) combining several advanced experimental techniques and state-of-the-art theoretical simulations. Both SAMs adopt dense, nested hexagonal structures but differ in their adsorption configurations and structural uniformity. While the **T2**-based SAM exhibits a low degree of order and noticeable deviation from the desired tripodal anchoring, all three anchoring groups of **T1** are equally bonded to the surface as thiolates, resulting in an almost upright orientation of the benzene rings and large-area structural uniformity. These superior properties are attributed to the effect of conformationally flexible methylene linkers at the anchoring groups, absent in the case of **T2**. Both SAMs display interesting electronic properties, and, bearing in mind that the triptycene framework can be functionalized by tail groups in various positions and with high degree of alignment, especially **T1** appears as an ideal docking platform for complex and highly functional molecular films.

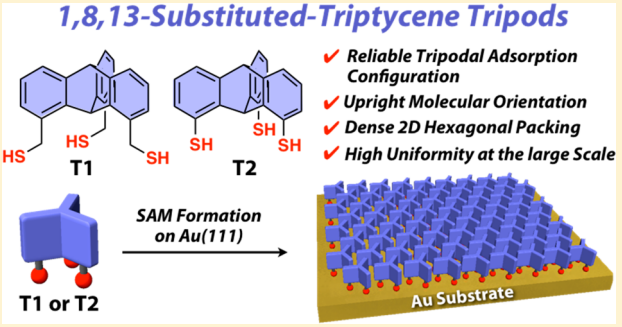

INTRODUCTION

Self-assembled monolayers (SAMs) enable tailoring the wettability, adhesiveness, and work-functions of solid substrates as well as organic/inorganic hybrid interfaces. As surfaces and interfaces typically determine the performance of devices especially at the nanoscale, the application of SAMs is of particular technological importance. Besides conventional monodentate SAMs with a single anchor group, several types of molecular platforms with multiple anchoring sites have recently been developed. This aims at more effectively controlling the orientation, spatial and lateral arrangement, and density of the molecules bonded to solid surfaces. Moreover, multiple anchoring groups help in achieving a robust anchoring configuration.[1] Of particular interest in this context are molecular tripods that usually consist of rigid tetrahedral cores bearing three anchors, such as thiol groups for binding to Au(111).[2−22] Examples for such systems include triarylmethane-based molecular tripods featuring an sp^3-hybridized carbon[4−8] or silicon[9−13] core (**A** and **B** in Figure 1a). Also, a methylene thiol-appended adamantane-based tripod (**C** in Figure 1a)[14−17] has been reported to form a hierarchical chiral network structure on Au(111).[15] Recently, Mayor et al.[4] investigated the impact of the configuration of anchor groups on the surface adsorption behavior, by comparing triarylmethane-based molecular tripods with *meta*-

Received: January 29, 2019
Published: March 14, 2019

DOI: 10.1021/jacs.9b00950
J. Am. Chem. Soc. 2019, 141, 5995−6005

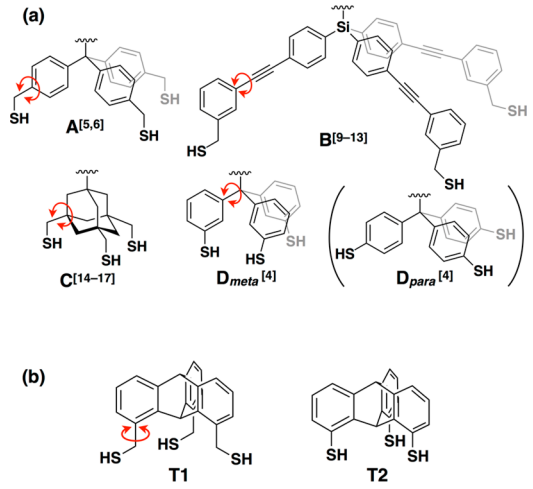

Figure 1. (a) Schematic structures of selected examples of reported molecular tripods (**A**–**D**). (b) Chemical structures of 1,8,13-substituted triptycene-based molecular tripods (**T1** and **T2**). Free rotation of the single bonds in **A**–**D**, highlighted by the curved red arrows, might result in anchoring groups pointing away from the substrate. In contrast, the three sulfur atoms of both **T1** and **T2** are arranged in a plane parallel to the triptycene independent of the conformation of the molecule, promoting three-point adsorption on a solid surface.

and *para*-type substitution patterns ($\mathbf{D}_{meta}$ and $\mathbf{D}_{para}$ in Figure 1a). They showed that the former can form covalently bonded monolayers on Au(111), while the latter only grow in multilayers.[4] This result underlines that careful molecular design of tripods is crucial for developing an optimal molecular platform for the controlled assembly on solid surfaces. Such a system should yield an adsorption state with all anchor groups equally bonded to the surface. Ideally, that would also result in a fully vertical molecular orientation. However, most existing molecular tripods adopt unfavorable conformations, where the anchor groups orient away from the surface due to free bond rotation of the sulfur-containing functionalities (as indicated by curved red arrows in Figure 1a). This leads to significant deviations from the desired tripodal anchoring configuration.

Herein, to overcome this problem and to develop an "ideal platform", we propose novel molecular tripods based on a highly rigid triptycene framework (Figure 1b). We have recently shown that 1,8,13-trisubstituted triptycenes exhibit superb self-assembling abilities to form well-defined, dense two-dimensional (2D) hexagonal structures through a nested packing of the aromatic blades.[23−28] This suggests that the trisubstituted triptycenes should offer a highly promising starting point for the development of ideal SAMs featuring well-controlled molecular density and orientation. Notably, due to the tridentate configuration, the present systems differ distinctly from previously reported monodentate triptycene-based monolayers with a single thiol or selenol group attached in the bridgehead position.[29,30] There, the triptycene moieties are prone to adopting a substantially tilted configuration.

In the present study, we synthesized two types of molecular tripods (Figure 1b) bearing anchoring thiol groups attached to the 1,8,13-positions of the triptycene framework either directly (**T2**) or via a methylene linker (**T1**). The former represents a rigid structure. All anchoring groups are located at fixed interthiol distances with the sulfur atoms in a plane parallel to the triptycene backbone. Notably, the interatomic distances between the sulfur atoms in **T2** quite closely fit the lattice structure of Au(111).[31] **T1** possesses a certain conformational flexibility due to the possibility of C−C bond-rotation in the thiol-containing functionality (Figure 1b, curved red arrow). Such a rotation allows adjusting the distances between the docking atoms without changing the plane in which the sulfur atoms are arranged. It also does not change the bonding geometry relative to the substrate, which for **T1** is different from that in **T2** due to the different inclination of the sulfur−carbon bonds. Overall, both **T1** and **T2** are designed to promote three-point adsorption on a solid surface.

A general advantage of triptycenes as anchoring platforms is that they can be substituted with functional units in various ways taking advantage of the four vacant sites per molecule, that is, the bridgehead,[25] 4, 5, and 16-positions.[24] To lay the foundations for the further development of triptycene-anchored SAMs, in the present study we focus on the self-assembly behavior of the fundamental triptycene-based tripods **T1** and **T2** on Au(111). For that, we use a variety of complementary experimental tools, including scanning tunneling microscopy (STM), X-ray photoelectron spectroscopy (XPS), near-edge X-ray absorption fine structure (NEXAFS) spectroscopy, and Kelvin probe (KP). The experimental findings are rationalized through dispersion-corrected density functional theory (DFT) simulations. We demonstrate that the triptycene-based tripods, especially **T1**, can adopt an adsorption configuration with (nearly) all thiol groups equivalently bonded to the substrate. Moreover, the **T1** molecules in the monolayers display an almost upright molecular orientation, an exceptionally high degree of order, and interesting electronic properties.

RESULTS AND DISCUSSION

Synthesis of T1 and T2. The synthesis of **T1** is illustrated in Scheme 1. The reaction of 1,8,13-trihydroxytriptycene (**3**)

Scheme 1. Synthesis of T1[a]

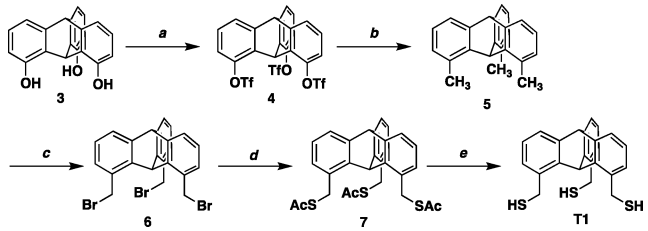

[a]Reagents and conditions: (a) Tf_2O, pyridine, 1,2-dichloroethane, 0–60 °C, 97%; (b) MeMgCl, Ni(dppp)Cl_2, THF, 80 °C, 80%; (c) NBS, AIBN, benzene, 50 °C, 59%; (d) AcSK, THF, 25 °C, 79%; (e) AcBr, MeOH, THF, −78 to 25 °C, 88%.

with triflic anhydride (Tf_2O) in the presence of pyridine gave tristriflate **4**,[24] which was converted into **5** by a Kumada–Tamao coupling reaction[32,33] using methylmagnesium chloride and Ni(dppp)Cl_2 (dppp = 1,3-bis(diphenylphosphino)-propane). Compound **5** was reacted with *N*-bromosuccinimide (NBS) in the presence of azobis(isobutyronitrile) (AIBN),[33] affording **6**. Treatment of **6** with potassium thioacetate (AcSK)[5,6] gave **7**, whose acetyl groups were hydrolyzed with HBr, which was generated in situ from acetyl bromide (AcBr) and MeOH,[34] to afford 1,8,13-trimercaptomethyltriptycene **T1**.[35]

DOI: 10.1021/jacs.9b00950
J. Am. Chem. Soc. 2019, 141, 5995−6005

1,8,13-Trimercaptotriptycene **T2** was synthesized from **3** according to Scheme 2. The hydroxyl groups of **3** were

Scheme 2. Synthesis of T2[a]

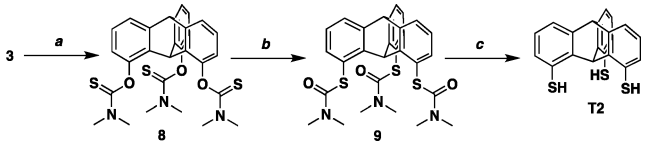

[a]Reagents and conditions: (a) NaH, *N*,*N*-dimethylthiocarbamoyl chloride, DMF, 0−70 °C, 83%; (b) Ph_2O, 260 °C, 84%; (c) KOH, MeOH, THF, 80 °C, 88%.

acylated with *N*,*N*-dimethylthiocarbamoyl chloride in the presence of NaH[36] to give **8**. Upon heating of **8** at 260 °C in diphenyl ether, the Newman−Kwart rearrangement[36] occurred to afford **9**. The carbamoyl groups of **9** were hydrolyzed with KOH in a mixture of MeOH and THF, resulting in **T2**. Compounds **T1** and **T2** were unambiguously characterized by ^{1}H and ^{13}C NMR spectroscopy, by FT-IR spectroscopy, and by high-resolution APCI-TOF mass spectrometry (Figures S18−S22 and Figures S30−S33 for **T1** and **T2**, respectively; see the Supporting Information). Successful preparation of single crystals of **T1** suitable for X-ray analysis allowed us to further determine the molecular structure of **T1** (Figure S1; see the Supporting Information).

Preparation of SAMs of T1 and T2 on Au(111). Standard thermally evaporated Au(111) substrates were used. SAMs of **T1** (**T1**/Au) and **T2** (**T2**/Au) were fabricated by simply immersing Au(111) substrates into a degassed THF solution of **T1** and **T2** for 24 h at 25 °C. The samples then were washed with THF, dried under ambient conditions, and annealed at 120 °C. Further details are provided in the Experimental Section. As a reference sample for the spectroscopic analysis, we also prepared benzylthiol (**B1**) SAMs on Au(111) using a standard procedure.[37]

STM Imaging of T1/Au and T2/Au SAMs. Large-area (50 nm × 50 nm) STM images of **T1**/Au (Figure 2a) and **T2**/Au (Figure 2b) both show smooth and homogeneous terraces with steps of ca. 2.5 Å, which is consistent with the well-known interlayer spacing at Au terraces on the surface of Au(111). This observation suggests that **T1** and **T2** cover the Au(111) surface uniformly. Close-up views (10 nm × 10 nm) of **T1**/Au (Figure 2c) and **T2**/Au (Figure 2d), which focus on a terrace, are very similar to one another and display hexagonally aligned bright spots at ca. 5 Å separation, indicating that both **T1** and **T2** self-assemble on Au(111) to form highly ordered domains. We assume that the bright spots stem from the phenyl rings of the triptycene units (as their most conductive parts directly linked to the substrate via the anchor groups). Thus, the **T1** and **T2** molecules on Au(111) likely assemble into a 2D nested hexagonal structure (Figure 2e), which is consistent with the packing of 1,8,13-trialkoxytriptycenes observed in X-ray diffraction experiments.[23−28] Consequently, also the centers of the phenyl groups align hexagonally with a separation of ca. 5 Å. From that, a packing density of the thiolate groups of 4.6 × 10^{14} thiolates/cm^2 can be calculated (Table 1).

XPS and NEXAFS Analysis of T1/Au and T2/Au SAMs. By means of XPS and NEXAFS spectroscopy, we further characterized **T1**/Au and **T2**/Au SAMs in terms of the sulfur−Au bonding state, packing density, orientation, and configuration of the triptycene molecules. Figure 3 shows

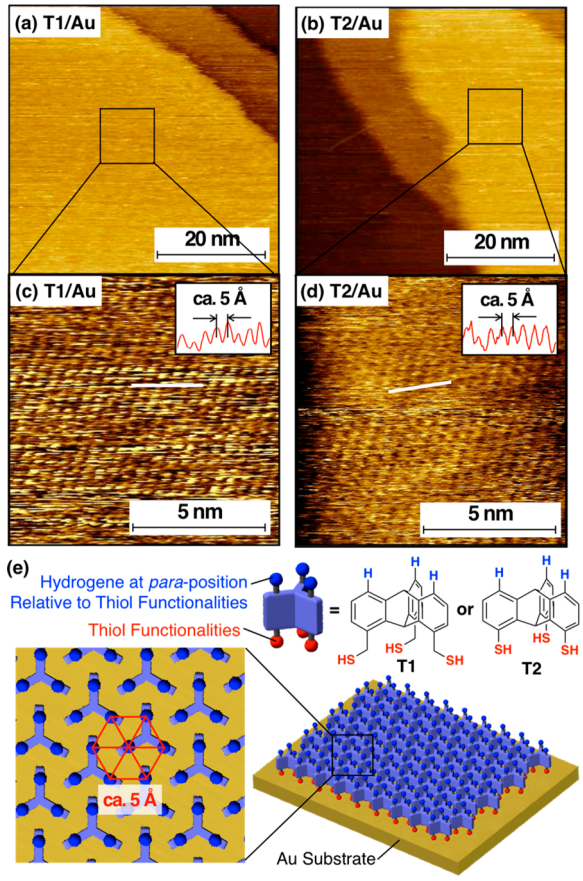

Figure 2. STM images of (a,c) **T1**/Au and (b,d) **T2**/Au acquired at 25 °C, and (e) schematic illustration of the proposed molecular arrangement of **T1** and **T2** on Au(111).

representative S 2p (Figure 3a−c) and C 1s (Figure 3d−f) XP spectra of **T1**/Au and **T2**/Au, along with those of **B1**/Au as a reference. The S 2p spectrum of **T1**/Au (Figure 3a) is very similar to that of **B1**/Au (Figure 3c): It is dominated by a characteristic S 2p doublet of thiolate bound to Au (Figure 3a, doublet 1) at ∼162.0 eV (S $2p_{3/2}$), with an only small (∼10%) admixture of an additional feature at 161.0 eV (S $2p_{3/2}$).[38] This suggests that almost all "legs" of the triptycene molecules in **T1**/Au are bound to the Au substrate as thiolates. This is an exceptionally good result for tripod-type molecules, which usually exhibit multiple bonding geometries with a significant portion of unbound and weakly bound anchoring groups.[4,39,40] The small feature at 161.0 eV (Figure 3a, doublet 2) is frequently observed in high-resolution XP spectra of thiolate-based SAMs[38] and is also present in the reference **B1**/Au SAM (Figure 3c). It can be attributed either to an anchoring configuration differing from a thiolate or, more likely, to atomic sulfur bound to the substrate, as discussed in detail in ref 38. Note that a small amount of atomically bound sulfur should not disturb the molecular packing, as the thiolate groups are quite loosely packed on the surface (see below).

The S 2p spectrum of **T2**/Au is also dominated by a characteristic S 2p doublet of thiolate bound to Au (Figure 3b, doublet 1). However, this spectrum contains noticeable contributions associated with physisorbed/unbound thiols (Figure 3b, doublet 3; ∼163.4 for S $2p_{3/2}$) and oxidized thiol groups (Figure 3b, doublet 4; ∼167.5 for S $2p_{3/2}$). The latter feature corresponds to sulfonate, which is the most commonly

DOI: 10.1021/jacs.9b00950
J. Am. Chem. Soc. 2019, 141, 5995−6005

Table 1. Observed and Calculated Effective Thickness, Packing Density of the Thiolate Groups, Average Tilt Angle of the π Plane (α), Average Molecular Tilt Angle (β), Work-Function Changes ($\Delta\Phi$), and Position of the Calculated XPS Peaks (Binding Energy) of T1/Au, T2/Au, and B1/Au

		packing density/10^{14} (thiolate/cm^2)			average tilt angle of π plane α (deg)[a]		average molecular tilt angle β (deg)[a]		work-function change $\Delta\Phi$ (eV)[b]		binding energy (eV)	
system	effective thickness (Å)	STM	XPS	calcd[c]	NEXAFS	calcd	NEXAFS	calcd	Kelvin probe	calcd	XPS	calcd
T1/Au	9	4.6	4.6	4.5	81	86.8	7.5	3.4	−0.80	−1.33	284.5	284.47
T2/Au	10.5	4.6	4.1	4.5	67	85.1	36	6.7	−0.75	−1.73	284.1	284.11
B1/Au	7		3.7	4.5	80	77.4	10	14.0			284.1	284.00

[a]The tilt angle refers to the orientation of the phenyl rings with respect to the substrate normal. See text for details. The experimental errors are ±1−1.5 Å for the thickness, ±10% for the packing density, and ±3° for the average tilt angle. [b]In the simulations, work-function changes are reported relative to a calculated work-function of a relaxed Au surface of 5.13 eV. [c]The slightly smaller value of the simulated packing density is a consequence of using the calculated Au lattice constants for reasons discussed in the Experimental Section.

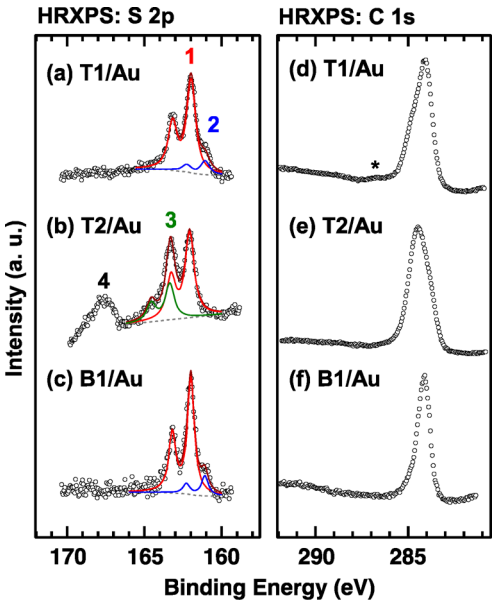

Figure 3. (a−c) S 2p and (d−f) C 1s XP spectra of **T1**/Au (a,d), **T2**/Au (b,e), and **B1**/Au (c,f) SAMs. Individual doublets in the S 2p spectra are color-coded and marked by numbers (see text for details); background is shown by gray dashed line.

observed oxidized species in thiolate SAMs,[1,38,41−43] that bonds only weakly to the substrate. For the spectrum presented in Figure 3b, the portions of the physisorbed/unbound thiols and sulfonate sulfur were estimated to be ∼15% and ∼20%, respectively. Thus, as compared to **T1**/Au, **T2**/Au exhibits a more heterogeneous bonding structure with some of the "legs" being only weakly bound, not bound, or oxidized.

The C 1s XP spectra of **T1**/Au (Figure 3d), **T2**/Au (Figure 3e), and **B1**/Au (Figure 3f) exhibit only one peak at 284.1, 284.5, and 284.1 eV, respectively. No contributions related to contaminations or oxidized species are observed, except for the spectrum of **T1**/Au, in which a very weak signal (asterisk) at ∼286.5 eV probably due to CO[44] is perceptible. While the peak in the spectrum of **B1**/Au is symmetric, the C 1s peaks for **T1**/Au and **T2**/Au display some asymmetry, with a higher intensity at the low binding-energy side for **T1**/Au and the opposite situation for **T2**/Au.

A quantitative analysis of the XP spectra (for details, see the Experimental Section) provides information on the effective thickness of the SAMs and the packing density of the thiolate groups. The results are listed in Table 1. The packing density of the thiolate groups determined by the XPS analysis of **T1**/Au (4.6×10^{14} thiolate/cm^2)[45] agrees perfectly with the estimate from the STM imaging. It corresponds to the ideal value of ca. one S atom per $\sqrt{3} \times \sqrt{3}$ surface unit cell and is also found for high-quality alkanethiolate SAMs on Au(111).[1] This testifies to the ideal surface coverage in the **T1**/Au system. For **T2**/Au, the average coverage derived from the XPS data (4.1×10^{14} thiolate/cm^2) is somewhat smaller. The area-averaging character of the XPS measurements, in combination with the higher local coverage observed for **T2**/Au in the STM images, suggest the coexistence of densely packed and more defective (i.e., less densely packed) areas in **T2**/Au. Notably, all determined packing densities for the triptycene-based SAMs are distinctly higher than that of the reference **B1** system (3.7×10^{14} thiolate/cm^2), underlining their superior quality. Consistently, the effective thickness of **T1**/Au is slightly higher than that of the reference **B1**/Au SAM (Table 1). The even higher effective thickness of **T2**/Au, despite the lower density of thiolate groups, is attributed to the presence of some physisorbed molecules.

NEXAFS spectroscopy experiments provided further insight into the structural quality of the SAMs and the molecular orientation. Representative data in Figure 4 comprise spectra acquired at the so-called magic angle of X-ray incidence (55°). They are independent of the molecular orientation and, thus, exclusively display the electronic structure of the SAMs.[46] Additionally, the differences between the spectra acquired under normal (90°) and grazing (20°) incidence are shown. They provide information on the molecular orientation.[46]

The 55° spectra of **T1**/Au (Figure 4a) and **T2**/Au (Figure 4c) are similar to one another and also do not significantly deviate from the spectrum of **B1**/Au (Figure 4e) and from reported spectra of oligophenyl SAMs in general.[47] They are dominated by the intense π_1* resonance of phenyl rings (Figure 4a, peak 1), which, however, appears at a slightly higher photon energy (∼285.3 eV) than for benzene (∼285.0 eV)[48] or oligophenyl SAMs (285.0−285.1 eV)[47] or even for triptycene SAMs with monodentate bonding configuration (∼285 eV).[30] We attribute that shift to a destabilization of the lowest unoccupied orbital in the triptycenes due to minor distortions of the phenyl rings by the central bridge, but, obviously, the tridentate bonding configuration is of importance as well. Additional low intensity resonances of oligophenyl SAMs, such as the R*/C−S* resonance at ∼287.3 eV and the π_2* resonance at 288.8−288.9 eV (Figure 4c, peak 2), are also resolved in spectra.[47] They are marginally smeared out for **T1**/Au and **T2**/Au, presumably due to their overlap with the features stemming from the sp^3 carbons at the

DOI: 10.1021/jacs.9b00950
J. Am. Chem. Soc. 2019, 141, 5995−6005

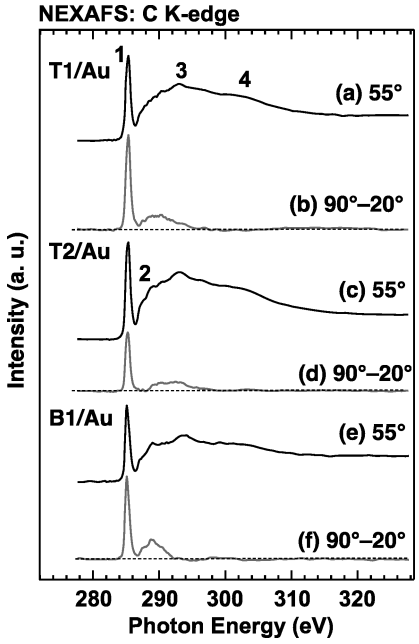

Figure 4. C K-edge NEXAFS data for the **T1**/Au (a,b), **T2**/Au (c,d), and **B1**/Au SAMs (e,f). They comprise the spectra acquired at an X-ray incidence angle of 55° (a,c,e) and the difference between the spectra acquired at X-ray incidence angles of 90° and 20° (b,d,f). Characteristic absorption resonances are marked by numbers (see text for details). Horizontal dashed lines in the difference spectra correspond to zero.

bridgehead positions. In addition, the spectra exhibited a variety of σ^*-like resonances (Figure 4a, peaks 3 and 4) at higher excitation energies.

The 90°−20° NEXAFS spectra of **T1**/Au, **T2**/Au, and **B1**/Au exhibit pronounced linear dichroism (Figure 4b,d,f) with the effect being particularly strong for the π_1^* resonances of the phenyl rings (Figure 4a, peak 1). In view of the specific orientation of the respective orbitals (perpendicular to the ring plane), a positive sign of the π_1^* difference peaks suggests upright molecular orientation of the phenyl rings relative to the substrate. This geometry corresponds to a predominantly downward orientation of the anchoring groups, allowing efficient anchoring of the triptycene tripods to the substrate, in full agreement with the conclusions from the XPS data.

A quantitative analysis of the NEXAFS data was performed within the commonly applied theoretical framework,[46] relying on the most prominent π_1^* resonance. To that aim, we correlated the dependence of its intensity on the incidence angle of the X-ray beams (θ) with a theoretical expression for a vector-like orbital,[46] using the average tilt angle of the π_1^* orbitals (α)[49] as the sole fitting parameter. The resulting values of α are 81°, 67°, and 80° for the **T1**/Au, **T2**/Au, and **B1**/Au, respectively (Table 1). Because of the 3-fold symmetry of **T1** and **T2**, the average value of the molecular tilt angle (β) can be directly obtained from the dependence of the intensity of the π_1^* resonance on $\cos^2\theta$.[30] The resulting values of β are shown in Table 1, along with the value for the **B1**/Au SAM. The latter can, however, only be considered as a lower limit of the average tilt angle in that system due to the lower molecular symmetry, which results in a dependence of the calculated value of β on the molecular twist (here set to 0° yielding the minimum value of β for a given α).[50]

The average value of β for **T1**/Au is quite small (~7.5°), suggesting that the benzene blades of **T1** are almost perpendicular to the substrate, which agrees well with the identical adsorption mode of all three anchoring groups (Table 1). The deviation from the fully parallel orientation could be explained by a possible corrugation of the specific anchoring sites of the three thiolate groups. This is, however, not supported by the simulations (see below). Therefore, we rather attribute it to a (small) number of defects, for example, at domain boundaries or step edges, and to the grain structure of the substrate within the macroscopically large area probed by NEXAFS spectroscopy.

For **T2**/Au, the average value of β is noticeably higher (Table 1), reflecting the lower quality of this monolayer as compared to **T1**/Au. This does not necessarily mean that **T2**/Au SAM contains no highly ordered areas of well-aligned molecules (see, e.g., STM experiments). These domains, however, must then coexist with areas of inhomogeneously bound and probably even physisorbed molecules with a strongly inclined or even stochastic orientation. This notion is consistent with the interpretation of the S 2p XP spectra and the derived coverages discussed above.

Computational Studies on the Structures of T1/Au and T2/Au. To gain atomistic insight into the properties of the **T1**/Au(111) and **T2**/Au(111) SAMs, we performed dispersion-corrected density-functional theory (DFT) calculations on periodic, infinitely extended interfaces. To be consistent with the experimental situation, we generated densely packed SAMs by choosing a 3 × 3 Au surface unit cell containing one molecule. This results in a hexagonal arrangement of triptycene molecules (Figure 5a,b) with a packing density of 4.45×10^{14} thiolate/cm^2 consistent with the experimental values.[51] The length of the resulting surface unit-

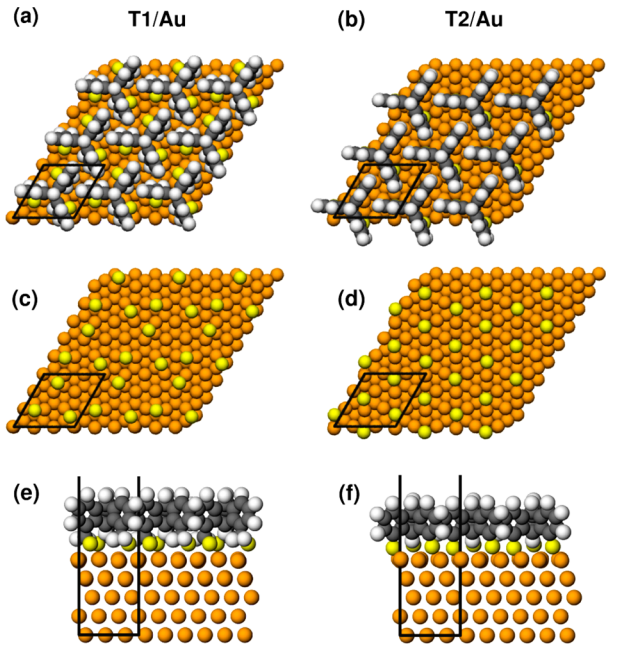

Figure 5. DFT-optimized structures of **T1**/Au (a and e; top and side views, respectively) and **T2**/Au (b and f; top and side views, respectively) on a 5-layer Au(111) slab and anchoring positions of the thiolate groups of **T1** (c) and **T2** (d). Only the S atoms and the Au slab are shown. The black rectangles represent the unit cell of the interfaces.

DOI: 10.1021/jacs.9b00950
J. Am. Chem. Soc. 2019, 141, 5995−6005

cell vectors is 8.82 Å,[52] which is somewhat larger than the unit-cell vector in the bulk assemblies of tripodal triptycenes, such as 1,8,13-tridodecyloxytriptycene (8.1 Å).[23−28] This difference arises from the fact that the dimensions of the surface unit cell are determined by the periodicity of the Au substrate, while the periodicity in the bulk reflects the optimum intrinsic distance for a hexagonal assembly of triptycene molecules. Consequently, one can expect some strain in the adsorbate layer, which might be one of the reasons for the structural imperfections found particularly for **T2** (without flexible methyl linkers).

A screening of possible anchoring sites for the densely packed monolayers yields S atoms located on the bridge sites shifted toward fcc hollow positions in the case of **T1**/Au and S atoms at fcc-hollow sites in **T2**/Au (Figure 5a,b). This is consistent with the computational results for isolated adsorbed molecules on Au(111).[31] The difference in anchoring sites is clearly visible in Figure 5c,d, where only the S atoms on the Au(111) surface are shown. The site in **T1**/Au corresponds to the ideal anchoring position typically found when simulating thiolate-bonded SAMs on Au(111) using a methodology similar to the present one.[53,54] The occurrence of a supposedly less ideal anchoring site in **T2**/Au is attributed to the structural rigidity of **T2**. It enforces an unusual arrangement of the S−C bonds nearly perpendicular to the Au surface, with the actual values of the angles between the bonds and the surface normal varying between 0.7° and 3.4°. The unusual thiolate bonding geometry results in some distortions of the molecular structure of **T2** upon adsorption, with the distance between neighboring S atoms increasing by 0.2 Å as compared to an isolated molecule. For **T2**/Au also the heights of the three docking groups vary quite significantly (between 0.61 and 1.03 Å relative to the topmost Au layer), while they are essentially the same (1.16 Å) for all S atoms in **T1**/Au (see Figure 5e and f). Consistent with the less ideal bonding configuration of **T2**/Au, the binding energy per molecule (representative of breaking the bond between the substrate and the adsorbate) is significantly smaller than that for **T1**/Au (5.43 eV vs 7.16 eV). A similar trend is observed for the adsorption energy characteristic of bond formation (1.62 eV vs 2.67 eV).

Simulated structural parameters for the absorbed molecules are summarized in Table 1. The tilt angle of the π_1* orbitals (α) and the molecular tilt angles (β) for **T1**/Au are 86.8° and 3.4°, respectively, which is in good agreement with the NEXAFS results (α = 81° and β = 7.5°). Conversely, the simulated values for well-ordered **T2**/Au (α = 85.1° and β = 6.7°) differ significantly from the NEXAFS values (α = 67° and β = 36°). As indicated already earlier, we attribute that to the coexistence of ordered and disordered domains in **T2**/Au, with essentially upright-standing molecules (β = 7.5°) in the ordered regions separated by severely disordered structures in between (see discussion of S 2p XP spectra).

Electronic Properties of the Interface. Functionalization of metal surfaces with SAMs is useful for tailoring the electronic properties of metal substrates.[55−59] Here, the triptycene-based SAM systems have a particularly high potential as surface modifier, because of the following: (i) They form dense and ordered monolayers with, in the case of **T1**, essentially upright-standing molecules. (ii) They can be efficiently chemically modified with various (polar) functional groups at the SAM−ambient interface at the 4,5,16-[24] and bridgehead positions.[25] To establish the basis for future applications, we here discuss experimental and theoretical investigations of the electronic properties of the "parent" interfaces **T1**/Au and **T2**/Au.

Kelvin-probe experiments on **T1**/Au and **T2**/Au yield work-functions (Φ) of 4.40 and 4.45 eV, respectively. With a Φ value of a bare, freshly sputtered Au(111) substrate of 5.20 eV,[60] this results in work-function modifications ($\Delta\Phi$) of −0.80 eV (for **T1**) and −0.75 eV (for **T2**). These values are comparable to those obtained for biphenylthiolate monolayers on Au(111) (Φ = 4.35−4.42 eV).[61]

As Kelvin probe is an area-averaging technique, the similarity in the final work-function of **T1**/Au and **T2**/Au might seem surprising considering the much higher degree of disorder in the **T2**/Au films. Disorder ought to result in much less ideally aligned dipoles and, consequently, a distinctly reduced work-function modification. As this is not observed, we conclude that for an ideally arranged **T2**/Au interface, much larger work-function changes than for **T1**/Au should be observed.

To test this hypothesis, we resorted to the simulations, which describe the situation of two perfectly ordered monolayers: The calculated work-function modification for **T1**/Au ($\Delta\Phi$ = −1.33 eV) somewhat overestimates the experimental value. This is in line with what we typically observe for polar SAMs[59] and can partly be attributed to the residual disorder in the experiments caused by step edges and grain boundaries. Additionally, the calculated molecular dipoles and bond dipoles are influenced by the employed computational methodology (see the Supporting Information). In line with the value for **T1**/Au, we calculate a work-function change of −1.38 eV for the biphenylthiolate SAM. In sharp contrast to those two cases, for a perfectly ordered **T2**/Au interface a much larger value of $\Delta\Phi$ = −1.73 eV is obtained, as expected on the basis of the arguments in the previous paragraph.

What remains to be explained is why the intrinsic work-function change for a **T2**/Au interface is by ca. 0.4 eV larger than that for **T1**/Au. To clarify that, we performed the following test: We modeled benzylthiolate (**B1**) and benzenethiolate (**B2**) SAMs, which differ only in the presence of a methyl linker between the phenyl and the thiolate in the former system. A full geometry optimization for both systems results in structures with the S atoms in bridge position shifted toward fcc-hollow sites (i.e., consistent with the situation for **T1**/Au). This yields a slightly larger work-function change of −1.44 eV for **B2**/Au as compared to −1.33 eV for **B1**/Au. When the S atom of the **B2** molecule is fixed at the fcc-hollow position (i.e., the favorable position for **T2**), the $\Delta\Phi$ value for **B2**/Au increased to −1.52 eV. When additionally fixing the position of the C atom bonded to the thiolate to the position it assumes in **T2**/Au, $\Delta\Phi$ rises further to −1.65 eV. This shows that the difference in $\Delta\Phi$ between **T2**/Au and **T1**/Au arises from the different hybridization states of the C atom bonded to the thiolate (sp^2 vs sp^3 hybridized) and, even more importantly, from differences in the C−S−Au bonding geometries.

A more local view of the electrostatics of the SAMs can be gained from an in-depth analysis of the XPS data.[62,63] The calculated C 1s XP spectra of **T1**/Au and **T2**/Au at a photon energy of 350 eV are reported in Figure 6. The energies scale is shifted by 18.88 eV in both systems[61,62] to align the experimental and calculated maxima for **T1**/Au. Fully consistent with the experiments, the positions of the peak maxima in the calculations differ by 0.4 eV between **T1**/Au (Figure 6a, 284.1 eV) and **T2**/Au (Figure 6b, 284.5 eV). The

DOI: 10.1021/jacs.9b00950
J. Am. Chem. Soc. 2019, 141, 5995−6005

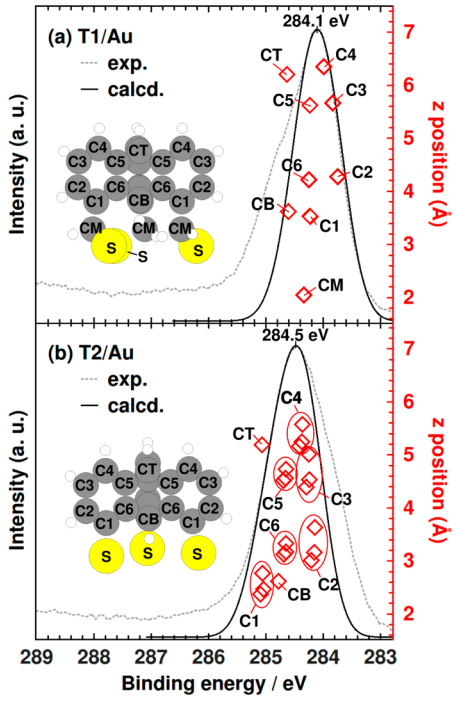

Figure 6. Simulated C 1s XP spectra of **T1**/Au (a) and **T2**/Au (b) for a primary photon energy of 350 eV. The contributions of the different groups of chemically equivalent C atoms are also shown, where the vertical position represents their z coordinates with respect to the image plane position (0.9 Å above the average z position of the topmost Au layer).

magnitude of that difference is close to the shift in $\Delta\Phi$ between the simulated **T1**/Au and **T2**/Au interfaces. As shifts in the electrostatic energy directly impact core-level binding energies,[62] this further supports the notion that for perfectly ordered SAMs the interfacial dipoles are larger in the **T2**/Au case. The reason why the electrostatic shift is resolved in the XPS experiments despite the disordered regions is that binding energies are impacted by the local electrostatic potential at the position of the excited atom such that variations of the electrostatic potential do not average out.[63] Figure 6 also shows the energetic positions of the C 1s core levels of the individual C atoms in the SAMs, which allows a direct comparison between **T1**/Au and **T2**/Au on an atom by atom level. Obviously, beyond the global shift between the spectra, the differences in binding energies between **T1**/Au and **T2**/Au are small for electrons from equivalent C atoms, except for CB and C1 carbons (see insets in Figure 6a,b). This confirms the earlier conclusion that differences in electrostatic energies and work-functions in the two SAMs originate from the immediate anchoring region.

CONCLUSIONS

Combining experimental and computational studies, we have demonstrated that triptycene-based molecular tripods (**T1** and **T2**) with thiol-containing functionalities at the 1,8,13-positions self-assemble into dense, uniform, and ordered monolayers on a metal surface with an upright orientation of the benzene planes. The key of the molecular design of **T1** and **T2** is that the three thiol groups are attached to a rigid triptycene framework in a way that they can efficiently bond to a surface, irrespective of possible conformational states. Moreover, 1,8,13-substituted triptycenes have a strong tendency to adopt nested 2D hexagonal structures, which promotes the self-assembly process.

The synthesis of **T1** and **T2** is achieved by sequential organic transformations from 1,8,13-trihydroxytriptycene in good overall yields. STM imaging of **T1** and **T2** assembled on Au(111) suggests the formation of uniform self-assembled monolayers (SAM) with an ordered 2D hexagonal arrangement of the triptycenes. On the basis of our XPS data, we conclude that (nearly) all of the S atoms of **T1** bind to Au(111). This results in an upright orientation of the molecules, as confirmed by NEXAFS measurements and quantum-mechanical simulations with a measured (calculated) tilt angle of 7.5° (3.4°). Conversely, the SAM of **T2** may contain significant amounts of unbound or weakly bound thiol groups, which causes partial oxidation of the thiol functionality. The large average tilt angle of 36° of **T2** on Au(111) determined by NEXAFS spectroscopy in combination with the STM, XPS, and modeling results suggests the coexistence of well-ordered domains with essentially upright standing molecules and highly disordered regions. The lower structural quality of the **T2**/Au interface can be traced back to a less favorable bonding arrangement in the immediate interface region, which also results in lower binding energies. Interestingly, despite the significantly different degrees of order in the **T1** and **T2** SAMs, the changes in the area-averaged work-function caused by the SAMs are essentially the same for both interfaces (ca. −0.8 eV). On the basis of the simulations and the XPS experiments, this can be rationalized by a significantly larger change in the well-ordered regions of **T2**/Au caused mostly be the different bonding geometry, which is eventually diminished by smaller values for the disordered parts of the film.

The results presented in this study establish a new type of tripodal SAM, whose architecture is distinctly different from conventional monolayers of molecular tripods. The advantages of the triptycene system, particularly **T1**, are the reliable tripodal adsorption configuration, the efficient large-area uniform 2D self-assembly, and an almost ideal upright orientation of the benzene rings, projected to the attached functional groups. Importantly, the triptycene tripods can be readily decorated using the bridgehead[25] or the 4,5,16-positions.[24] As either one or three functional groups per tripod can then be substituted, their density and separation can readily be varied. Thus, the presented systems can serve as stable and conformationally rigid anchors, for example, for polar entities modifying sample work-functions, for recognition functionalities in combination with biomolecules, or for receptor groups in sensing applications. This makes them highly promising building blocks for applications in organic and molecular circuits, biomedical devices, optical and chemical sensors, solid catalyst, and many more.

EXPERIMENTAL SECTION

Materials. Unless otherwise stated, all commercial reagents were used as received. Benzylthiol (**B1**) and hexadecanethiol (HDT) were purchased from Sigma-Aldrich. Compound **3** was prepared according to previously reported procedures[23] and unambiguously characterized by nuclear magnetic resonance (NMR) spectroscopy and atmospheric pressure chemical ionization time-of-flight (APCI-TOF) mass spectrometry. For long-term storage of **T1** and **T2**, these compounds were stored under an argon or nitrogen atmosphere in the freezer to avoid oxidation of the thiol groups.

General. NMR spectroscopy measurements were carried out on a Bruker AVANCE-500 spectrometer (500 MHz for ^{1}H and 125 MHz

DOI: 10.1021/jacs.9b00950
J. Am. Chem. Soc. 2019, 141, 5995−6005

for ^{13}C) or AVANCE-400 spectrometer (400 MHz for ^{1}H and 100 MHz for ^{13}C). Chemical shifts (δ) are expressed relative to the resonances of the residual nondeuterated solvents for ^{1}H [$CDCl_3$, $^{1}H(\delta)$ = 7.26 ppm; acetone-d_6, $^{1}H(\delta)$ = 2.05 ppm] and ^{13}C [$CDCl_3$, $^{13}C(\delta)$ = 77.16 ppm; acetone-d_6, $^{13}C(\delta)$ = 29.8 and 206.3 ppm]. Absolute values of the coupling constants are given in Hertz (Hz), regardless of their sign. Multiplicities are abbreviated as singlet (s), doublet (d), triplet (t), multiplet (m), and broad (br) (see the Supporting Information). Infrared (IR) spectra were recorded at 25 °C on a JASCO FT/IR-6600ST Fourier-transform infrared spectrometer. High-resolution mass spectrometry measurements were carried out on a Bruker micrOTOF II mass spectrometer equipped with an atmospheric pressure chemical ionization (APCI) probe or an electrospray ionization (ESI) probe.

STM Measurements. STM tips were mechanically cut from a tungsten wire (diameter 0.25 mm; Nilaco). Au(111) substrates, obtained by thermal evaporation of Au onto a freshly cleaved mica substrate, were flame-annealed and quenched in ethanol prior to use. Samples for STM imaging were prepared by immersing an Au(111) substrate into a degassed THF solution (2.0 μ mol/L) of **T1** or **T2** for 24 h, and the resultant substrate was washed with THF, dried in air, and then thermally annealed (120 °C, 1 h) under reduced pressure. Constant current-mode STM imaging was carried out on a Nanoscope III STM system (Digital Instruments). All STM measurements were performed at 25 °C in air. The STM scanner was calibrated with an Au(111) substrate prior to the experiments. The observed STM contrast (apparent height) difference of 2.5 Å was consistent with the well-known interlayer separation at Au terraces on Au(111).

Preparation of SAMs for the Spectroscopy and Kelvin Probe Measurements. The SAMs for these experiments were prepared on commercial Au substrates (Georg Albert PVD, Silz, Germany). These substrates were prepared by thermal evaporation of 30 nm of Au (99.99% purity) onto a polished single-crystal silicon (100) wafer (Silicon Sense) that had been precoated with a 5 nm titanium adhesion layer. The resulting Au films are polycrystalline, having a grain size of 20−50 nm and predominantly exhibiting a (111) orientation. The SAMs were prepared by immersion of a fresh substrate in a degassed THF solution (2 μM−1 mM) of **T1** or **T2** for 24 h at 25 °C. After immersion, the films were washed with THF and dried by blowing argon. Finally, some of the samples were annealed at 100 °C for 1 h either under inert gas atmosphere or under ultrahigh vacuum (UHV) conditions. In addition, several reference SAMs, that is, those of **B1** and HDT on Au(111), were prepared using standard procedures.[37] HDT/Au was used as a reference system for the XPS and work-function measurements (see below). **B1** can be regarded as a partial structure of **T1**, making it a suitable monothiol reference. Because of the presence of the methylene linker between the benzene ring and thiol group, a sufficiently good quality of this monolayer can be expected, similar to the analogous nitrile-substituted system.[64] At the same time, we refrained from studying benzenethiol as the monothiol reference to **T2**, as it has been shown to form SAMs of only limited quality when employing the standard immersion procedure.[47,65]

XPS and NEXAFS Spectroscopy Measurements. The XPS, NEXAFS spectroscopy, and work-function measurements were performed under UHV conditions (1.5×10^{-9} mbar) at 25 °C.

Laboratory XPS measurements were carried out with a MAX200 (Leybold-Heraeus) spectrometer equipped with an Mg Kα X-ray source (200 W) and a hemispherical analyzer. The spectra were corrected for the spectrometer transmission, and the binding energy (BE) scale was referenced to the Au $4f_{7/2}$ peak at 84.0 eV.[44] Because the quality of the laboratory spectra in terms of statistics and energy resolution was inferior to the synchrotron data, they were mostly used to verify the film thickness and packing density.

Synchrotron-based XPS measurements were carried out at the bending magnet HE-SGM beamline of the synchrotron storage ring BESSY II in Berlin, Germany. This beamline provides a moderate X-ray intensity helping to avoid X-ray damage during the spectra acquisition. The spectra were collected with a Scienta R3000 electron energy analyzer in normal emission geometry. The photon energy (PE) was set to either 350 or 580 eV, depending on the BE range. The BE scale was referenced to the Au $4f_{7/2}$ peak at 84.0 eV.[44] The energy resolution was ∼0.3 eV at a PE of 350 eV and ∼0.5 at 580 eV.

The XPS data were used to calculate the effective thickness and packing density of the SAMs, relying on the C 1s/Au 4f and S 2p/Au 4f intensity ratios using standard procedures.[66,67] For the thickness evaluation, a standard expression for the attenuation of the photoemission signal was assumed[68] together with literature values for the attenuation lengths.[69] The spectrometer-specific coefficients were determined with the help of the reference HDT SAM with a known thickness (18.9 ± 0.1 Å) and packing density (4.63×10^{14} molecules/cm^2; $\sqrt{3} \times \sqrt{3}$ structure).[37]

NEXAFS spectroscopy measurements were performed at the same beamline. The spectra were collected at the C K-edge in the partial electron yield mode with a retarding voltage of −150 V. The polarization factor of the X-ray's was estimated as ∼88%; the energy resolution was ∼0.30 eV. The incidence angle of the light was varied from 90° (normal incidence geometry; **E**-vector in surface plane) to 20° (grazing incidence geometry; **E**-vector near surface normal) in steps of 10°−20°, which is a standard approach enabling the determination of the molecular orientation from NEXAFS data.[42] Raw spectra were normalized to the incident photon flux by division through a spectrum of a clean, freshly sputtered gold sample. The PE scale was referenced to the pronounced π^* resonance of highly oriented pyrolytic graphite at 285.38 eV.[70]

Kelvin Probe Measurements. Work-function measurements were carried out using a UHV Kelvin Probe 2001 system (KP technology Ltd., UK). The pressure in the UHV chamber was $\sim 10^{-9}$ mbar. As reference, we used HDT/Au with the work-function value set to 4.30 eV according to the literature.[71] The latter value was additionally verified by referencing it to the work-function of freshly sputtered gold set to 5.20 eV.[72] The accuracy of the WF values is ca. ±0.05 eV.

Computational Methodology. The calculations were performed using the FHI-aims code[73] and employing the PBE functional[74] in combination with the surface parametrization[75] of the Tkatchenko−Scheffler dispersion correction.[76] The latter were turned off between the bulk Au atoms. Periodic boundary conditions and the repeated slab approach including a vacuum region of at least 20 Å in the z direction were employed to represent the interface. To compensate for the electrostatic asymmetry of the slab, a self-consistently calculated dipole layer was inserted in the vacuum.[77] To sample the reciprocal space, a nonorthogonal $6 \times 6 \times 1$ Γ-centered k-point grid was used. The dimensions of the unit cells in the x and y directions were defined according to the calculated Au nearest neighbor distance (2.940 Å), to avoid spurious surface relaxations. The metal was modeled using 5 layers of Au, with the bottom 3 layers fixed at their bulk positions during the optimization. The presented results were obtained using the default FHI-aims "tight" basis set and setting the total energy criterion for the self-consistency cycle to 10^{-6} eV. The optimizations were performed until the maximum residual force component per atom was below 0.01 eV/Å. For the initial screening of different docking sites, less accurate settings were adopted, using the default FHI-aims "light" basis set and stopping the optimization when the maximum residual force component per atom was below 0.05 eV/Å.

Binding energies, E_{bind}, are defined such that they reflect the energy needed to break the bond between the molecule and the substrate and to remove the molecules from the SAM:

$$E_{bind} = E_{Trip/Au} - E_{Au} - E_{Trip} \quad (1)$$

Here, $E_{Trip/Au}$ is the energy per unit cell of the SAM adsorbed to the surface, E_{Au} is the energy of the optimized pristine Au slab, and E_{Trip} is the energy of the optimized gas-phase molecular radical. Conversely, adsorption energies, E_{ads}, reflect the energetics of forming the monolayers and at the same time replacing the molecular S−H bonds by bonds to the Au surface. They are, thus, defined as

$$E_{ads} = E_{Trip/Au} - E_{Au} - E_{Trip\text{-}H} + 3/2E_{H2} \quad (2)$$

DOI: 10.1021/jacs.9b00950
J. Am. Chem. Soc. 2019, 141, 5995−6005

E_{Trip-H} in this equation represents the energy of the optimized gas-phase triptycene molecule in which all S atoms are saturated with hydrogens, and E_{H2} is the energy of an isolated H_2 molecule.

The XP spectra were simulated within the initial state approach to avoid artifacts arising from a combination of periodic boundary conditions and explicit excitations in each unit cell.[62] For obtaining the spectra, the 1s core level energies for every C atom were taken from the atom projected density of states output files. Subsequently, they were shifted considering the screening of the core hole by the metal substrate via an electrostatic image charge model[78,79] assuming a dielectric constant of the SAM of 3.9.[80] To model the spectra, the individual resonances were broadened using Gaussian functions with a variance of 0.15 eV and an intensity scaled using an exponential attenuation function to account for the finite escape depth of the photoelectrons. Additionally, the energy scales for both interfaces were rigidly shifted by the same energy to align the calculated and measured positions of the C 1s peaks for **T1**/Au. This is inevitable, considering that when employing the initial state approach, Kohn–Sham orbital energies are calculated. For more details, see refs 61 and 62.

In the simulations of the benzylthiolate (**B1**) and benzenethiolate (**B2**) SAMs, two molecules per $(3 \times \sqrt{3})rect$ unit cell in a herringbone arrangement were considered. For that cell, we chose an orthogonal 9 × 5 × 1 Γ-centered *k*-point grid. When placing the molecules at specific adsorption sites, only the positions of the S atoms were fixed. All of the other were relaxed. When also fixing the molecular tilt, this was achieved by only fixing the coordinates of the C atom directly bonded to S.

■ ASSOCIATED CONTENT

Supporting Information

The Supporting Information is available free of charge on the ACS Publications website at DOI: 10.1021/jacs.9b00950.

Details of synthesis, NMR, IR, high-resolution MS spectra, single-crystal X-ray structural analysis, and computational details (PDF)

X-ray crystallographic data for **T1** (CIF)

■ AUTHOR INFORMATION

Corresponding Authors

*michael.zharnikov@urz.uni-heidelberg.de

*egbert.zojer@tugraz.at

*fukushima@res.titech.ac.jp

ORCID

Fumitaka Ishiwari: 0000-0002-0200-4510

Yoshiaki Shoji: 0000-0001-8437-1965

Shintaro Fujii: 0000-0003-2869-7674

Manabu Kiguchi: 0000-0002-8179-7466

Tomofumi Tada: 0000-0003-3093-3779

Egbert Zojer: 0000-0002-6502-1721

Takanori Fukushima: 0000-0001-5586-9238

Author Contributions

#F.I., G.N., and E.S. contributed equally.

Notes

The authors declare no competing financial interest.

■ ACKNOWLEDGMENTS

This work was supported by a Grant-in-Aid for Scientific Research on Innovative Areas "π-Figuration" (26102008 for T.F., 26102013 for M.K., and 26102017 for T.T.) of the Ministry of Education, Culture, Sports, Science, and Technology (MEXT), Japan, Grant-in-Aid for the Promotion of Joint International Research (15K21721) of MEXT, Japan, JST CREST (JPMJCR18I4 for T.F.), Japan, the German Research Foundation (Deutsche Forschungsgemeinschaft; DFG, grant ZH 63/22-1 for E.S. and M.Z.), and the Austrian Science Fund (FWF, I2081-N20 for G. N. and E.Z.). T.F. acknowledges support from the Dynamic Alliance for Open Innovation Bridging Human, Environment and Materials from MEXT, Japan. We thank Dr. Valiparambil Sanjayan Sajisha and Ms. K. Takenouchi for their assistance in the synthesis of **T1** and **T2**. We thank Suzukakedai Materials Analysis Division, Technical Department, Tokyo Institute of Technology, for their support with the NMR measurement and single-crystal X-ray analysis. E.S. and M.Z. thank the Helmholtz Zentrum Berlin for the allocation of synchrotron radiation beamtime at BESSY II and A. Nefedov and Ch. Wöll for the technical cooperation during the experiments there. The computational results have been achieved using the Vienna Scientific Cluster (VSC3).

■ REFERENCES

(1) Love, J. C.; Estroff, L. A.; Kriebel, J. K.; Nuzzo, R. G.; Whitesides, G. M. Self-Assembled Monolayers of Thiolates on Metals as a Form of Nanotechnology. *Chem. Rev.* **2005**, *105*, 1103–1169.

(2) Valášek, M.; Lindner, M.; Mayor, M. Rigid Multipodal Platforms for Metal Surfaces. *Beilstein J. Nanotechnol.* **2016**, *7*, 374–405.

(3) Valášek, M.; Mayor, M. Spatial and Lateral Control of Functionality by Rigid Molecular Platforms. *Chem. - Eur. J.* **2017**, *23*, 13538–13548.

(4) Lindner, M.; Valášek, M.; Homberg, J.; Edelmann, K.; Gerhard, L.; Wulfhekel, W.; Fuhr, O.; Wächter, T.; Zharnikov, M.; Kolivoška, V.; Pospíšil, L.; Mészáros, G.; Hromadová, M.; Mayor, M. Importance of the Anchor Group Position (Para versus Meta) in Tetraphenylmethane Tripods: Synthesis and Self-Assembly Features. *Chem. - Eur. J.* **2016**, *22*, 13218–13235.

(5) Hirayama, D.; Takimiya, K.; Aso, Y.; Otsubo, T.; Hasobe, T.; Yamada, H.; Imahori, H.; Fukuzumi, S.; Sakata, Y. Large Photocurrent Generation of Gold Electrodes Modified with [60]Fullerene-Linked Oligothiophenes Bearing a Tripodal Rigid Anchor. *J. Am. Chem. Soc.* **2002**, *124*, 532–533.

(6) Zhu, S.-E; Kuang, Y.-M.; Geng, F.; Zhu, J.-Z.; Wang, C.-Z.; Yu, Y.-J.; Luo, Y.; Xiao, Y.; Liu, K.-Q.; Meng, Q.-S.; Zhang, L.; Jiang, S.; Zhang, Y.; Wang, G.-W.; Dong, Z.-C.; Hou, J. G. Self-Decoupled Porphyrin with a Tripodal Anchor for Molecular-Scale Electroluminescence. *J. Am. Chem. Soc.* **2013**, *135*, 15794–15800.

(7) Nikitin, K.; Lestini, E.; Lazzari, M.; Altobello, S.; Fitzmaurice, D. A Tripodal [2]Rotaxane on the Surface of Gold. *Langmuir* **2007**, *23*, 12147–12153.

(8) Sakamato, R.; Ohirabaru, Y.; Matsuoka, R.; Maeda, H.; Katagiri, S.; Nishihara, H. Orthogonal Bis(terpyridine)–Fe(II) Metal Complex Oligomer Wires on a Tripodal Scaffold: Rapid Electron Transport. *Chem. Commun.* **2013**, *49*, 7108–7110.

(9) Chen, K.-Y.; Ivashenko, O.; Carroll, G. T.; Robertus, J.; Kistemaker, J. C. M.; London, G.; Browne, W. R.; Rudolf, P.; Feringa, B. L. Control of Surface Wettability Using Tripodal Light-Activated Molecular Motors. *J. Am. Chem. Soc.* **2014**, *136*, 3219–3224.

(10) Jian, H.; Tour, J. M. En Route to Surface-Bound Electric Field-Driven Molecular Motors. *J. Org. Chem.* **2003**, *68*, 5091–5103.

(11) Shirai, Y.; Cheng, L.; Cheng, B.; Tour, J. M. Characterization of Self-Assembled Monolayers of Fullerene Derivatives on Gold Surfaces: Implications for Device Evaluations. *J. Am. Chem. Soc.* **2006**, *128*, 13479–13486.

(12) Ramachandra, S.; Schuermann, K. C.; Edafe, F.; Belser, P.; Nijhuis, C. A.; Reus, W. F.; Whitesides, G. M.; De Cola, L. Luminescent Ruthenium Tripod Complexes: Properties in Solution and on Conductive Surfaces. *Inorg. Chem.* **2011**, *50*, 1581–1591.

(13) Chen, K.-Y.; Ivashenko, O.; Carroll, G. T.; Robertus, J.; Kistemaker, J. C. M.; London, G.; Browne, W. R.; Rudolf, P.; Feringa, B. L. Control of Surface Wettability Using Tripodal Light-Activated Molecular Motors. *J. Am. Chem. Soc.* **2014**, *136*, 3219–3224.

DOI: 10.1021/jacs.9b00950
J. Am. Chem. Soc. 2019, 141, 5995–6005

(14) Kitagawa, T.; Idomoto, Y.; Matsubara, H.; Hobara, D.; Kakiuchi, T.; Okazaki, T.; Komatsu, K. Rigid Molecular Tripod with an Adamantane Framework and Thiol Legs. Synthesis and Observation of an Ordered Monolayer on Au(111). *J. Org. Chem.* **2006**, *71*, 1362−1369.
(15) Katano, S.; Kim, Y.; Matsubara, H.; Kitagawa, T.; Kawai, M. Hierarchical Chiral Framework Based on a Rigid Adamantane Tripod on Au(111). *J. Am. Chem. Soc.* **2007**, *129*, 2511−2515.
(16) Kitagawa, T.; Matsubara, H.; Komatsu, K.; Hirai, K.; Okazaki, T.; Hase, T. Ideal Redox Behavior of the High-Density Self-Assembled Monolayer of a Molecular Tripod on a Au(111) Surface with a Terminal Ferrocene Group. *Langmuir* **2013**, *29*, 4275−4282.
(17) Kitagawa, T.; Matsubara, H.; Okazaki, T.; Komatsu, K. Electrochemistry of the Self-Assembled Monolayers of Dyads Consisting of Tripod-Shaped Trithiol and Bithiophene on Gold. *Molecules* **2014**, *19*, 15298−15313.
(18) Wagner, S.; Leyssner, F.; Kördel, C.; Zarwell, S.; Schmidt, R.; Weinelt, M.; Rück-Braun, K.; Wolf, M.; Tegeder, P. Reversible Photoisomerization of an Azobenzene-Functionalized Self-Assembled Monolayer Probed by Sum-Frequency Generation Vibrational Spectroscopy. *Phys. Chem. Chem. Phys.* **2009**, *11*, 6242−6248.
(19) Takamatsu, D.; Fukui, K.; Aroua, S.; Yamakoshi, Y. Photoswitching Tripodal Single Molecular Tip for Noncontact AFM Measurements: Synthesis, Immobilization, and Reversible Configurational Change on Gold Surface. *Org. Biomol. Chem.* **2010**, *8*, 3655−3808.
(20) Valášek, M.; Edelmann, K.; Gerhard, L.; Fuhr, O.; Lukas, M.; Mayor, M. Synthesis of Molecular Tripods Based on a Rigid 9,9'-Spirobifluorene Scaffold. *J. Org. Chem.* **2014**, *79*, 7342−7357.
(21) Šebera, J.; Kolivoška, V.; Valášek, M.; Gasior, J.; Sokolová, R.; Mészáros, G.; Hong, W.; Mayor, M.; Hromadová, M. Tuning Charge Transport Properties of Asymmetric Molecular Junctions. *J. Phys. Chem. C* **2017**, *121*, 12885−12894.
(22) Gerhard, L.; Edelmann, K.; Homberg, J.; Valášek, M.; Bahoosh, S. G.; Lukas, M.; Pauly, F.; Mayor, M.; Wulfhekel, W. An Electrically Actuated Molecular Toggle Switch. *Nat. Commun.* **2017**, *8*, 14672.
(23) Seiki, N.; Shoji, Y.; Kajitani, T.; Ishiwari, F.; Kosaka, A.; Hikima, T.; Takata, M.; Someya, T.; Fukushima, T. Rational Synthesis of Organic Thin Films with Exceptional Long-range Structural Integrity. *Science* **2015**, *348*, 1122−1126.
(24) Shioya, H.; Shoji, Y.; Seiki, N.; Nakano, M.; Fukushima, T.; Iwasa, Y. Raising the Metal−Insulator Transition Temperature of VO_2 Thin Films by Surface Adsorption of Organic Polar Molecules. *Appl. Phys. Express* **2015**, *8*, 121101.
(25) Leung, F. K.-C.; Ishiwari, F.; Kajitani, T.; Shoji, Y.; Hikima, T.; Takata, M.; Saeki, A.; Seki, S.; Yamada, Y. M. A.; Fukushima, T. Supramolecular Scaffold for Tailoring the Two-Dimensional Assembly of Functional Molecular Units into Organic Thin Films. *J. Am. Chem. Soc.* **2016**, *138*, 11727−11733.
(26) Yokota, T.; Kajitani, T.; Shidachi, R.; Tokuhara, T.; Kaltenbrunner, M.; Shoji, Y.; Ishiwari, F.; Sekitani, T.; Fukushima, T.; Someya, T. A Few-Layer Molecular Film on Polymer Substrates to Enhance the Performance of Organic Devices. *Nat. Nanotechnol.* **2018**, *13*, 139−144.
(27) Ishiwari, F.; Shoji, Y.; Fukushima, T. Supramolecular Scaffolds Enabling the Controlled Assembly of Functional Molecular Units. *Chem. Sci.* **2018**, *9*, 2028−2041.
(28) Ishiwari, F.; Okabe, G.; Ogiwara, H.; Kajitani, T.; Tokita, M.; Takata, M.; Fukushima, T. Terminal Functionalization with a Triptycene Motif that Dramatically Changes the Structural and Physical Properties of an Amorphous Polymer. *J. Am. Chem. Soc.* **2018**, *140*, 13497−13502.
(29) Liu, J.; Wachter, T.; Irmler, A.; Weidler, P. G.; Gliemann, H.; Pauly, F.; Mugnaini, V.; Zharnikov, M.; Woll, C. Electric Transport Properties of Surface-Anchored Metal-Organic Frameworks and the Effect of Ferrocene Loading. *ACS Appl. Mater. Interfaces* **2015**, *7*, 9824−9830.
(30) Liu, J.; Kind, M.; Schüpbach, B.; Käfer, D.; Winkler, S.; Zhang, W.; Terfort, A.; Wöll, C. Triptycene-Terminated Thiolate and Selenolate Monolayers on Au(111). *Beilstein J. Nanotechnol.* **2017**, *8*, 892−905.
(31) Tada, T.; Ishiwari, F.; Shoji, Y.; Fukushima, T. First-Principles Study of the Adsorption Behavior of Triptycene Molecular Tripods on Au(111): Site-Selectivity and Unambiguous Molecular Orientation. *J. Phys. Chem. C* **2019**, *123*, 4401−4406.
(32) Tamao, K.; Sumitani, K.; Kiso, Y.; Zembayashi, M.; Fujioka, A.; Kodama, S.; Nakajima, I.; Minato, A.; Kumada, M. Nickel-Phosphine Complex-Catalyzed Grignard Coupling. I. Cross-Coupling of Alkyl, Aryl, and Alkenyl Grignard Reagents with Aryl and Alkenyl Halides: General Scope and Limitations. *Bull. Chem. Soc. Jpn.* **1976**, *49*, 1958−1969.
(33) Ooi, T.; Kameda, M.; Maruoka, K. Design of *N*-Spiro C_2-Symmetric Chiral Quaternary Ammonium Bromides as Novel Chiral Phase-Transfer Catalysts: Synthesis and Application to Practical Asymmetric Synthesis of α-Amino Acids. *J. Am. Chem. Soc.* **2003**, *125*, 5139−5151.
(34) Kawauchi, T.; Oguchi, Y.; Nagai, K.; Iyoda, T. Conical Gradient Junctions of Dendritic Viologen Arrays on Electrodes. *Sci. Rep.* **2015**, *5*, 11122.
(35) Xiao, Y.; Mague, J. T.; Pascal, R. A., Jr An Exceptionally Close, Non-Bonded Hydrogen-Hydrogen Contact with Strong Through-Space Spin-Spin Coupling. *Angew. Chem., Int. Ed.* **2018**, *57*, 2244−2247.
(36) Lloyd-Jones, G. C.; Moseley, J. D.; Renny, J. S. Mechanism and Application of the Newman-Kwart O–>S Rearrangement of *O*-Aryl Thiocarbamates. *Synthesis* **2008**, *5*, 661−689.
(37) Schreiber, F. Structure and growth of self-assembling monolayers. *Prog. Surf. Sci.* **2000**, *65*, 151−256.
(38) Zharnikov, M. High-Resolution X-Ray Photoelectron Spectroscopy in Studies of Self-Assembled Organic Monolayers. *J. Electron Spectrosc. Relat. Phenom.* **2010**, *178−179*, 380−393.
(39) Park, J.-S.; Vo, A. N.; Barriet, D.; Shon, Y. S.; Lee, T. R. Systematic Control of the Packing Density of Self-Assembled Monolayers Using Bidentate and Tridentate Chelating Alkanethiols. *Langmuir* **2005**, *21*, 2902−2911.
(40) Weidner, T.; Ballav, N.; Siemeling, U.; Troegel, D.; Walter, T.; Tacke, R.; Castner, D. G.; Zharnikov, M. Tripodal Binding Units for Self-Assembled Monolayers on Gold: A Comparison of Thiol and Thioether Headgroups. *J. Phys. Chem. C* **2009**, *113*, 19609−19617.
(41) Hutt, D. A.; Leggett, G. J. Influence of Adsorbate Ordering on Rates of UV Photooxidation of Self-Assembled Monolayers. *J. Phys. Chem.* **1996**, *100*, 6657−6662.
(42) Hutt, D. A.; Cooper, E.; Leggett, G. J. Structure and Mechanism of Photooxidation of Self-assembled Monolayers of Alkylthiols on Silver Studied by XPS and Static SIMS. *J. Phys. Chem. B* **1998**, *102*, 174−184.
(43) Wang, M.-C.; Liao, J.-D.; Weng, C.-C.; Klauser, R.; Shaporenko, A.; Grunze, M.; Zharnikov, M. Modification of Aliphatic Monomolecular Films by Free Radical Dominant Plasma: The Effect of the Alkyl Chain Length and the Substrate. *Langmuir* **2003**, *19*, 9774−9780.
(44) Moulder, J. F.; Stickle, W. E.; Sobol, P. E.; Bomben, K. D. In *Handbook of X-ray Photoelectron Spectroscopy*; Chastian, J., Ed.; Perkin-Elmer Corp.: Eden Prairie, MN, 1992.
(45) The molecular packing densities in the Trip1S/Au and TripS/Au represent 1/3 of the values in Table 1, that is, 1.53×10^{14} and 1.37×10^{14} molecules/cm^2, respectively.
(46) Stöhr, J. *NEXAFS Spectroscopy*; Springer-Verlag: Berlin, 1992.
(47) Frey, S.; Stadler, V.; Heister, K.; Eck, W.; Zharnikov, M.; Grunze, M.; Zeysing, B.; Terfort, A. Structure of Thioaromatic Self-Assembled Monolayers on Gold and Silver. *Langmuir* **2001**, *17*, 2408−2415.
(48) Horsley, J.; Stöhr, J.; Hitchcock, A. P.; Newbury, D. C.; Johnson, A. L.; Sette, F. Resonances in the K Shell Excitation Spectra of Benzene and Pyridine: Gas Phase, Solid, and Chemisorbed States. *J. Chem. Phys.* **1985**, *83*, 6099−6107.
(49) The definitions of α and β of **T1** and **T2** are identical to those in ref 30.

DOI: 10.1021/jacs.9b00950
J. Am. Chem. Soc. 2019, 141, 5995−6005

(50) Ballav, N.; Schüpbach, B.; Dethloff, O.; Feulner, P.; Terfort, A.; Zharnikov, M. Direct Probing Molecular Twist and Tilt in Aromatic Self-Assembled Monolayers. *J. Am. Chem. Soc.* **2007**, *129*, 15416−15417.
(51) The slightly smaller value arises from using the calculated lattice constant of Au rather than the experimental one.
(52) The lattice constant is calculated to be 8.65 Å when employing the experimental bulk lattice constant of Au at room temperature instead of the calculated one.
(53) Felice, R. D.; Selloni, A.; Molinari, E. DFT Study of Cysteine Adsorption on Au(111). *J. Phys. Chem. B* **2003**, *107*, 1151−1156.
(54) Gottschalk, J.; Hammer, B. A Density Functional Theory Study of the Adsorption of Sulfur, Mercapto, and Methylthiolate on Au(111). *J. Chem. Phys.* **2002**, *116*, 784−790.
(55) Campbell, I. H.; Rubin, S.; Zawodzinski, T. A.; Kress, J. D.; Martin, R. L.; Smith, D. L.; Barashkov, N. N.; Ferraris, J. P. Controlling Schottky Energy Barriers in Organic Electronic Devices Using Self-Assembled Monolayers. *Phys. Rev. B: Condens. Matter Mater. Phys.* **1996**, *54*, 14321−14324.
(56) Heimel, G.; Romaner, L.; Zojer, E.; Bredas, J.-L. The Interface Energetics of Self-Assembled Monolayers on Metals. *Acc. Chem. Res.* **2008**, *41*, 721−729.
(57) Alloway, D. M.; Hofmann, M.; Smith, D. L.; Gruhn, N. E.; Graham, A. L.; Colorado, R.; Wysocki, V. H.; Lee, T. R.; Lee, P. A.; Armstrong, N. R. Interface Dipoles Arising from Self-Assembled Monolayers on Gold: UV-Photoemission Studies of Alkanethiols and Partially Fluorinated Alkanethiols. *J. Phys. Chem. B* **2003**, *107*, 11690−11699.
(58) de Boer, B.; Hadipour, A.; Mandoc, M. M.; van Woudenbergh, T.; Blom, P. W. M. Tuning of Metal Work Functions with Self-Assembled Monolayers. *Adv. Mater.* **2005**, *17*, 621−625.
(59) Abu-Husein, T.; Schuster, S.; Egger, D. A.; Kind, M.; Santowski, T.; Wiesner, A.; Chiechi, R.; Zojer, E.; Terfort, A.; Zharnikov, M. The Effects of Embedded Dipoles in Aromatic Self-Assembled Monolayers. *Adv. Funct. Mater.* **2015**, *25*, 3943−3957.
(60) Derry, G. N.; Kern, M. E.; Worth, E. H. Recommended Values of Clean Metal Surface Work Functions. *J. Vac. Sci. Technol., A* **2015**, *33*, 060801.
(61) M. Gärtner, M.; Sauter, E.; Nascimbeni, G.; Petritz, A.; Wiesner, A.; Kind, M.; Abu-Husein, T.; Bolte, M.; Stadlober, B.; Zojer, E.; Terfort, A.; Zhanikov, M. Tailor-Made Self-Assembled Monolayers with Embedded Dipole Moments for Interface Engineering in Organic Electronics. *J. Phys. Chem. C* **2018**, *122*, 28757−28774.
(62) Taucher, T. C.; Hehn, I.; Hofmann, O. T.; Zharnikov, M.; Zojer, E. Understanding Chemical versus Electrostatic Shifts in X-Ray Photoelectron Spectra of Organic Self-Assembled Monolayers. *J. Phys. Chem. C* **2016**, *120*, 3428−3437.
(63) Hehn, I.; Schuster, S.; Wächter, T.; Abu-Husein, T.; Terfort, A.; Zharnikov, M.; Zojer, E. Employing X-ray Photoelectron Spectroscopy for Determining Layer Homogeneity in Mixed Polar Self-Assembled Monolayers. *J. Phys. Chem. Lett.* **2016**, *7*, 2994−3000.
(64) Hamoudi, H.; Neppl, S.; Kao, P.; Schüpbach, B.; Feulner, P.; Terfort, A.; Allara, D.; Zharnikov, M. Orbital-Dependent Charge Transfer Dynamics in Conjugated Self-Assembled Monolayers. *Phys. Rev. Lett.* **2011**, *107*, 027801.
(65) Shaporenko, A.; Terfort, A.; Grunze, M.; Zharnikov, M. A Detailed Analysis of the Photoemission Spectra of Basic Thioaromatic Monolayers on Noble Metal Substrates. *J. Electron Spectrosc. Relat. Phenom.* **2006**, *151*, 45−51.
(66) Thome, J.; Himmelhaus, M.; Zharnikov, M.; Grunze, M. Increased Lateral Density in Alkanethiolate Films on Gold by Mercury Adsorption. *Langmuir* **1998**, *14*, 7435−7449.
(67) Chesneau, F.; Schüpbach, B.; Szelagowska-Kunstman, K.; Ballav, N.; Cyganik, P.; Terfort, A.; Zharnikov, M. Self-Assembled Monolayers of Perfluoroterphenyl-Substituted Alkanethiols: Specific Characteristics and Odd−Even Effects. *Phys. Chem. Chem. Phys.* **2010**, *12*, 12123−12127.
(68) Ratner, M.; Castner, D. Electron Spectroscopy for Chemical Analysis. In *Surface Analysis−The Principal Techniques*; Vickerman, J., Ed.; Wiley: Chichester, 1997.
(69) Lamont, C. L. A.; Wilkes, J. Attenuation Length of Electrons in Self-Assembled Monolayers of *n*-Alkanethiols on Gold. *Langmuir* **1999**, *15*, 2037−2042.
(70) Batson, P. E. Carbon 1s Near-Edge-Absorption Fine Structure in Graphite. *Phys. Rev. B: Condens. Matter Mater. Phys.* **1993**, *48*, 2608−2610.
(71) Cabarcos, O. M.; Schuster, S.; Hehn, I.; Zhang, P. P.; Maitani, M. M.; Sullivan, N.; Giguère, J.-B.; Morin, J.-F.; Weiss, P. S.; Zojer, E.; Zharnikov, M.; Allara, D. L. Effects of Embedded Dipole Layers on Electrostatic Properties of Alkanethiolate Self-Assembled Monolayers. *J. Phys. Chem. C* **2017**, *121*, 15815−15830.
(72) Ford, W. E.; Gao, D.; Knorr, N.; Wirtz, R.; Scholz, F.; Karipidou, Z.; Ogasawara, K.; Rosselli, S.; Rodin, V.; Nelles, G.; von Wrochem, F. Organic Dipole Layers for Ultralow Work Function Electrodes. *ACS Nano* **2014**, *8*, 9173−9180.
(73) Blum, V.; Gehrke, R.; Hanke, F.; Havu, P.; Havu, V.; Ren, X.; Reuter, K.; Scheffler, M. *Ab Initio* Molecular Simulations with Numeric Atom-Centered Orbitals. *Comput. Phys. Commun.* **2009**, *180*, 2175−2196.
(74) Perdew, J. P.; Burke, K.; Ernzerhof, M. Generalized Gradient Approximation Made Simple. *Phys. Rev. Lett.* **1996**, *629*, 453−462.
(75) Ruiz, V. G.; Liu, W.; Zojer, E.; Scheffler, M.; Tkatchenko, A. Density-Functional Theory with Screened van der Waals Interactions for the Modeling of Hybrid Inorganic-Organic Systems. *Phys. Rev. Lett.* **2012**, *108*, 146103.
(76) Tkatchenko, A.; Scheffler, M. Accurate molecular van der Waals interactions from Ground-State Electron Density and Free-Atom Reference Data. *Phys. Rev. Lett.* **2009**, *102*, 073005.
(77) Freysoldt, C.; Eggert, P.; Rinke, P.; Schindlmayr, A.; Scheffler, M. Screening in Two Dimensions: GW Calculations for Surfaces and Thin Films using the Repeated-Slab Approach. *Phys. Rev. B: Condens. Matter Mater. Phys.* **2008**, *77*, 214517.
(78) Jackson, J. D. *Classical Electrodynamics*, 3rd ed.; Wiley: New York, 1999.
(79) Neaton, J.; Hybertsen, M.; Louie, S. Renormalization of Molecular Electronics Levels at Metal-Molecules Interfaces. *Phys. Rev. Lett.* **2006**, *97*, 216405.
(80) Levstik, A.; Filipič, C.; Levstik, I. Dielectric properties of Biphenyl. *J. Phys.: Condens. Matter* **1990**, *2*, 3031−3033.

DOI: 10.1021/jacs.9b00950
J. Am. Chem. Soc. 2019, 141, 5995−6005